J. Fluid Mech. (2008), *vol.* 595, *pp.* 461–490.
doi:10.1017/S0022112007009512 Printed in the United Kingdom

Instability of an oscillatory fluid layer with insoluble surfactants

PENG GAO AND XI-YUN LU†

Department of Modern Mechanics, University of Science and Technology of China, Hefei, Anhui 230026, China

(Received 28 January 2007 and in revised form 8 October 2007)

The linear stability of an infinite fluid layer with a deformable free surface covered by an insoluble surfactant and bounded below by a horizontal rigid plate oscillating in its own plane is studied based on the Floquet theory. The differential system governing the stability problem for perturbations of arbitrary wavenumbers is solved numerically by a Chebyshev collocation method. Stability boundaries are obtained in a wide range of amplitude and frequency of the modulation as well as surfactant elasticity. Results show that the presence of the surfactant may significantly stabilize (destabilize) the flow by raising (lowering) the critical Reynolds number associated with the onset of instability. The effect of the surfactant plays a stabilizing role for small surfactant elasticity and a destabilizing one for relatively large surfactant elasticity. The destabilizing effect of the surfactant on the stability of flows with a zero-shear surface is found for the first time. The disturbance modes in the form of travelling waves may be induced by the surfactant and dominate the instability of the flow.

1. Introduction

The stability of a fluid layer adjacent to walls is of considerable theoretical interest and has a variety of applications, such as coating, crystal growth and materials processing. In a majority of previous studies on the stability of films, the basic flow configuration is usually treated as a steady system. However, unsteadiness usually occurs and may play an important role in flow behaviours. For example, residual vibrations are always unavoidable and cause instability (Skarda 2001; Thiele, Vega & Knobloch 2006), which may be critical to manufactured product quality. Thus, the relevant stability studies, e.g. stability of a fluid layer driven by an oscillating plane, and stability of film flow with surfactant, are desirable.

The flow of a fluid layer driven by a plate oscillating in its own plane is a typical problem for studying the stability of periodic flows with a free surface. Yih (1968) performed a linear stability analysis of this flow in the limit of long-wave disturbances. An analytical expression of the growth rate was obtained using perturbation theory, that may be regarded as an extension of the method for the stability of steady flows (Yih 1963), and a disturbance mode associated with the surface deformation was identified. The stability of the flow depends on the Froude number F and a dimensionless parameter β, related to the modulation frequency. The long-wave disturbances may be unstable only on certain separated bandwidths of the imposed

† Author to whom correspondence should be addressed: xlu@ustc.edu.cn

frequency. The instabilities, if they exist, occur for sufficiently large amplitude of modulation in the presence of gravity and for any non-zero amplitude in the absence of gravity. By extending the long-wave analysis of Yih (1968), the linear stability of the same flow with arbitrary wavenumbers was further studied by Or (1997). The differential system was solved numerically based on Floquet theory. A new type of instability related to finite-wavelength disturbances occurs when the Reynolds number R exceeds a threshold. The curves in the (R, β)-plane, indicating the variation of the critical Reynolds number for finite-wavelength instability, branch off a family of open-ended loops corresponding to the long-wave stability boundaries of Yih (1968), and fill the gap of the imposed frequency where long-wave modes are stable. Moreover, some parts of the long-wave stability boundaries are not associated with criticality owing to the competition of the finite-wavelength instabilities. Both the long- and finite-wavelength neutral modes are synchronous with the modulation and evolve in the form of standing waves. In related work, Or & Kelly (1998) also performed a linear stability analysis of the flow with the combined effect of oscillatory shear and themocapillarity.

For two-fluid oscillating flow systems, Coward & Papageorgiou (1994) considered the long-wave stability of a periodic Couette flow confined between two plates, with one of them oscillating with time. The instability owning to the viscosity stratification can be either stabilized or destabilized by the oscillations. Similar conclusions were also obtained by Coward & Renardy (1997) in studying a periodic two-layer Couette–Poiseulle flow. The linear stability of oscillatory two-fluid Couette flow was also investigated by King, Leighton & McCready (1999). In addition to a linear stability analysis, the interfacial instability was also studied experimentally between two concentric cylinders. Both theoretical and experimental results agree well with each other. Halpern & Frenkel (2001) studied the nonlinear stability of an oscillatory Couette film flow, focusing on the density stratification.

The instability of the oscillatory free surface is strongly controlled by the surface tension, which is usually assumed to be uniform. The surface tension may be very sensitive to the presence of surface-active agents or surfactants, which may play an important role in free-surface problems (e.g. Sarpkaya 1996; Shen, Yue & Triantafyllou 2004). The variation of the surfactant concentration induces a spatial gradient of the surface tension and accompanying Marangoni traction, leading to an additional disturbance flow field in the fluid layer. This disturbance flow together with the perturbations in the basic velocity profile in turn affects the deflection of the surface on the one hand, and causes local accumulation and the dilution of the surfactant by the advective effects on the other hand. This closed-loop process results in different stability characteristics of the flow compared with the cases in the absence of the surfactant.

It is believed that the presence of an insoluble surfactant has a stabilizing effect on the stability of single-fluid systems, which are usually accompanied by a zero-shear free surface. For gravity-driven film flows down an inclined or vertical wall, the most dangerous mode has an asymptotical zero wavenumber (Yih 1963). Whitaker& Jones (1966) and Lin (1970) performed a long-wave analysis for the stability of surfactant-laden films and found that the critical Reynolds number associated with the Yih mode was raised, indicating a stabilizing effect of the surfactants. Pozrikidis (2003) examined the same problem for perturbations of arbitrary wavenumbers but in the limit of vanishing Reynolds number, and found another so-called Marangoni mode due to the presence of the surfactant, in addition to the Yih mode associated with the surface deflection. The rate of decay of the Marangoni mode is less than

that of the Yih mode for any wavenumber, so that the presence of the surfactant is regarded as destabilizing in this sense. Blyth & Pozrikidis (2004*a*) carried out a stability analysis of a surfactant-covered film flow by numerically solving the Orr–Sommerfeld equation for finite Reynolds number. They found that the variation of the Reynolds number hardly affects the growth rates of the Marangoni mode, which is always damped. Thus, the criticality is still determined by the growth of the Yih mode which is suppressed by the surfactant.

Some studies have demonstrated a destabilizing influence of an insoluble surfactant on the interface with a non-zero shear. Frenkel & Halpern (2002) performed a long-wave stability analysis of two-fluid channel flows and revealed for the first time an interfacial instability induced solely by an insoluble surfactant. This instability occurs even in the limit of Stokes flow and disappears in the absence of the surfactant. The surfactant-induced instabilities for perturbations of arbitrary wavenumbers were also detected in their subsequent work devoted to the same problem (Halpern & Frenkel 2003). These findings were confirmed by Blyth & Pozrikidis (2004*b*), who proposed an analysis of the two-fluid channel flow using a lubrication-flow model and extended the stability analysis into the nonlinear regime. The effect of small inertia on the surfactant-induced instability was addressed in Frenkel & Halpern (2005). Since a necessary condition for the occurrence of the Marangoni instability in Frenkel & Halpern (2002) and Halpern & Frenkel (2003) is the non-zero interfacial shear of the basic flow, Wei (2005*a*) studied the long-wave stability of a single-fluid film flow down an inclined plane by imposing an additional surface shear stress and found that the flow could indeed be destabilized by the presence of an insoluble surfactant. Both stabilizing and destabilizing effects of insoluble surfactants on the instability of a two-layer film flow were detected by Gao & Lu (2007).

The linear stabilities of both falling film and two-fluid channel flow systems were revisited by Wei (2005*b*). Two coupled evolution equations for the interface deformation and surfactant concentration in the limit of long waves and negligible inertia were derived. The equations for both the systems have similar forms. Thus, why the presence of the surfactant is stabilizing in one case but destabilizing in another is explained using the same framework. In addition, Wei (2005*b*) presented an argument that the existence of an interface shear of the basic flow is not essential for the existence of the surfactant-induced instability.

Although the stabilities of steady film flows in the presence of surfactants have been extensively investigated, the effects of an insoluble surfactant on the stability of an oscillatory fluid layer seem to have been overlooked in previous studies. To our knowledge, the only work is Wei, Halpern & Grotberg (2005), who investigated the linear stability of surfactant-covered core–annular film flow driven by a periodic pressure gradient through a capillary. We performed a long-wave stability analysis of an oscillatory film flow with the surfactant effect (Gao & Lu 2006*a*), and found that unstable regions in the parameter space shrink owing to the introduction of the surfactant, indicating a stabilizing Marangoni effect. The main purpose of the present study is to investigate how the finite-wavelength instability of the flow is affected by the presence of surfactants, and to demonstrate that an oscillatory free surface may be destabilized by the surfactants.

This paper is organized as follows. The physical problem and the mathematical formulations for the linear stability analysis are defined in § 2. Numerical methods for solving the governing equations with arbitrary wavenumbers are presented in § 3. Detailed results are given in § 4 and some concluding remarks are addressed in § 5.

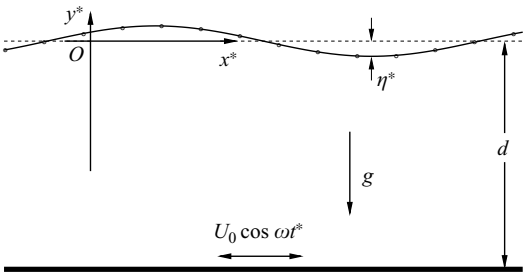

FIGURE 1. Schematic illustration of the flow configuration.

2. Problem definition and formulations

We consider the flow of a horizontal layer of incompressible Newtonian fluid with the density ρ and viscosity μ (figure 1). The fluid layer is bounded below by an infinite horizontal plate, which oscillates in the x^*-direction with velocity $U_0 \cos \omega t^*$, where U_0 is the amplitude of the oscillation and ω is the modulation frequency. Here and below we use an asterisk to denote dimensional variables. The upper surface is deformable and is covered by a monolayer of insoluble surfactant. Let $\boldsymbol{v}^* = (u^*, v^*)$ represent the fluid velocity, with u^* and v^* being the velocity components in the horizontal and vertical directions, respectively. Then the motion of the fluid is governed by the Navier–Stokes equation and the continuity equation

$$\frac{\partial \boldsymbol{v}^*}{\partial t^*} + \boldsymbol{v}^* \cdot \nabla \boldsymbol{v}^* = -\frac{1}{\rho} \nabla p^* + \nu \nabla^2 \boldsymbol{v}^* + \boldsymbol{g}, \tag{2.1}$$

$$\nabla \cdot \boldsymbol{v}^* = 0, \tag{2.2}$$

where $\nabla = (\partial/\partial x^*, \partial/\partial y^*)$, p^* is the hydrodynamic pressure, $\nu = \mu/\rho$ is the kinematic viscosity and $\boldsymbol{g}$ represents the acceleration due to gravity.

The free surface of the fluid layer is described by $y^* = \eta^*(x^*, t^*)$, and covered by a monolayer of insoluble surfactant with concentration $\Gamma^*(x^*, t^*)$, which is convected and diffuses over the surface. The governing equation of motion of the surfactant in moving curvilinear coordinates has been given in previous work (Stone 1990; Wong, Rumschitzki & Maldarelli 1996; Li & Pozrikidis 1997). Since only the two-dimensional stability problem is considered here, we use the one-dimensional transport equation for surfactant obtained by Halpern & Frenkel (2003). Hence the surfactant concentration $\Gamma^*(x^*, t^*)$ obeys

$$\frac{\partial (H\Gamma^*)}{\partial t^*} + \frac{\partial}{\partial x^*}(H\Gamma^* u^*) = D_s \frac{\partial}{\partial x^*}\left(\frac{1}{H}\frac{\partial \Gamma^*}{\partial x^*}\right), \tag{2.3}$$

where $H = \sqrt{1 + \eta_{x^*}^{*2}}$ and D_s is the surfactant diffusivity. Owing to the presence of the surfactant, the surface tension γ^* will depend on the local surfactant concentration and hence varies in space and time. Since we are concerned with infinitesimal perturbations to study the linear stability of the flow, the relation between the surface tension γ^* and the surfactant concentration Γ^* can be approximated as

$$\gamma^* = \gamma_0 - E(\Gamma^* - \Gamma_0), \tag{2.4}$$

where E is a constant denoting the surface elasticity, and Γ_0 is the basic value of the surfactant concentration, corresponding to a uniform surface tension γ_0. It is necessary to indicate that γ_0 is different from the surface tension in the absence of surfactant.

The velocity field should satisfy the no-slip boundary condition at the plate. At the free surface, we apply the kinematic boundary condition and the dynamic condition requiring the balance of the hydrodynamic traction, the surface tension, and the Marangoni traction (e.g. Pozrikidis 2003; Blyth & Pozrikidis 2004*a*).

We choose the amplitude of the wall velocity U_0 as the characteristic scale of velocity, the mean thickness of the film d as the scale of length, ω^{-1} as the scale of time, and ρU_0^2 as the scale of pressure. The surfactant concentration and surface tension are normalized by Γ_0 and γ_0, respectively. Then, in the basic state, the surface is flat, $\eta = 0$, and the surfactant concentration and surface tension are uniform, $\Gamma = \gamma = 1$. According to Gao & Lu (2006*a*), the dimensionless form of the basic streamwise velocity profile is given by

$$U(y,t) = \mathrm{Re}\left[\frac{\cosh(1+\mathrm{i})\beta y}{\cosh(1+\mathrm{i})\beta}\mathrm{e}^{\mathrm{i}t}\right], \quad -1 \leqslant y \leqslant 0, \tag{2.5}$$

where $\beta = \sqrt{\omega d^2/2\nu}$ is the ratio of the mean thickness of the film to the thickness of the Stokes layer induced by wall oscillation, and is also interpreted as a measure of the oscillation frequency. The basic pressure, induced by gravity, is represented as

$$P(y) = -\frac{2\chi}{R^2}y, \quad -1 \leqslant y \leqslant 0, \tag{2.6}$$

where the Galileo number $\chi = gd^3/2\nu^2$ is the ratio of gravity force to viscous force, and $R = U_0 d/\nu$ is the Reynolds number.

According to Gao & Lu (2006*a*), the motion of infinitesimal disturbances with wavenumber k is governed by the time-dependent Orr–Sommerfeld equation

$$\left(2\beta^2\frac{\partial}{\partial t} + \mathrm{i}kRU\right)\left(\frac{\partial^2}{\partial y^2} - k^2\right)\phi - \mathrm{i}kRU_{yy}\phi = \left(\frac{\partial^2}{\partial y^2} - k^2\right)^2\phi, \tag{2.7}$$

with ϕ being the complex amplitude of the disturbance streamfunction. The boundary conditions at the wall are

$$\phi = \frac{\partial\phi}{\partial y} = 0 \quad \text{at} \quad y = -1. \tag{2.8}$$

The linearized versions of the boundary conditions at the surface as well as the kinematic condition and the surfactant transport equation are

$$2\beta^2\frac{\partial^2\phi}{\partial t\,\partial y} - \left(\frac{\partial^2}{\partial y^2} - 3k^2 - \mathrm{i}kRU\right)\frac{\partial\phi}{\partial y} + \frac{1}{R}\left(2\chi + \frac{k^2}{\psi}\right)\mathrm{i}kh = 0, \tag{2.9}$$

$$\frac{\partial^2\phi}{\partial y^2} + k^2\phi + U_{yy}h + \frac{Ma}{\psi R}\mathrm{i}k\xi = 0, \tag{2.10}$$

$$2\beta^2\frac{\mathrm{d}h}{\mathrm{d}t} + \mathrm{i}kRUh + \mathrm{i}kR\phi = 0, \tag{2.11}$$

$$2\beta^2\frac{\mathrm{d}\xi}{\mathrm{d}t} + \mathrm{i}kRU\xi + \mathrm{i}kR\frac{\partial\phi}{\partial y} + \frac{k^2}{Pe}\xi = 0, \tag{2.12}$$

evaluated at $y = 0$, where h and ξ are the complex amplitudes of the disturbances to the surface and surfactant concentration, respectively.

The additional non-dimensional parameters in the free-surface conditions are defined as

$$\psi = \frac{\rho\nu^2}{\gamma_0 d}, \quad Ma = \frac{E\Gamma_0}{\gamma_0}, \quad Pe = \frac{U_0 d}{D_s}. \tag{2.13}$$

The parameter ψ measures the surface tension. Ma is the Marangoni number, representing the sensitivity of the surface tension on the surfactant concentration. Pe is the Péclet number, indicating the strength of convective to diffusive transport of surfactant; actually, the surfactant diffusion is usually negligible and hence is discarded below, i.e. $Pe^{-1} = 0$. Therefore, together with β, R and χ, we have five dimensionless parameters to characterize the stability of the flow. These parameters are convenient for the analysis of the finite-wavelength instability, and have been used by Or (1997) to study the stability of a fluid layer with a clean surface. We employ them here in order to compare our results with those of Or (1997). Furthermore, an appealing feature of these parameters is that the effects of the modulation amplitude and frequency, which are of interest in the present study, are measured solely by R and β. The effects of gravity and surface tension are involved in χ and ψ, respectively. Instead, for the long-wavelength instability analysis (Yih 1968; Gao & Lu 2006*a*), the Froude number F and the capillary number Ca are convenient. They are defined and related to the current parameters by

$$F^{-2} = \frac{gd}{U_0^2} = \frac{2\chi}{R^2}, \qquad Ca = \frac{\mu U_0}{\gamma_0} = \psi R. \tag{2.14}$$

In addition, a non-dimensional group

$$M = \frac{Ma}{\psi R^2}, \tag{2.15}$$

is suitable for characterizing the effect of surfactants on the long-wavelength instability of the flow (Gao & Lu 2006*a*), and is retained for the arbitrary-wavelength analysis here, so that the long-wavelength portions of the results may remain unchanged for fixed values of M instead of Ma.

Since U is periodic in t, the time-dependent Orr–Sommerfeld equation (2.7) subject to conditions (2.8) to (2.12) forms a Floquet system, which governs the linear stability of the flow. According to the Floquet theory, the solutions of the system can be reasonably expressed by

$$[\phi(y,t), h(t), \xi(t)] = \mathrm{e}^{\mu t}[\hat{\phi}(y,t), \hat{h}(t), \hat{\xi}(t)], \tag{2.16}$$

where the eigenfunctions $\hat{\phi}(y,t)$, $\hat{h}(t)$ and $\hat{\xi}(t)$ are 2π-periodic in time, the same as the basic velocity U; the Floquet exponent $\mu = \mu_r + \mathrm{i}\mu_i$, has a real part, μ_r, representing the growth rate of the disturbance in the sense of an average over one period and an imaginary part, μ_i, leading to a quasi-periodic motion of the disturbance. Since $\mu_r + \mathrm{i}(\mu_i + n)$, for any integer n, is also an eigenvalue, μ_i can be confined for definiteness on the interval $(-1/2, 1/2]$. The basic flow is unstable if there exists at least one Floquet exponent μ, with positive real part, i.e. $\mu_r > 0$, corresponding to an exponential growth of the disturbance. The stability of the flow is then determined by the eigenrelation

$$\mu = \mu(k; R, \beta, \psi, \chi, M), \tag{2.17}$$

which serves to relate the complex Floquet exponent, μ, to the disturbance wavenumber, k, for specified values of other parameters. For long-wavelength perturbations, i.e. $k \ll 1$, the Floquet modes, which are responsible for the instability of the flow, can be obtained analytically by an expansion in k (Gao & Lu 2006*a*). However, for finite-wavelength instabilities, the differential system should be solved numerically.

For the stability considered here, there exists a useful symmetry property of the solution to the differential system (2.7) to (2.12). Translating the time by π and taking the complex conjugate of the system, we can find that (2.7) remains formally invariant, and the differences lie in the boundary conditions that the signs of those terms involving h and ξ in (2.8) to (2.12) are reversed. It means that if $\phi(y,t)$, $h(t)$ and $\xi(t)$ are the solutions, then so are $\widetilde{\phi}(y,t+\pi)$, $-\widetilde{h}(t+\pi)$ and $-\widetilde{\xi}(t+\pi)$, where a tilde denotes the complex conjugate. Accordingly, as will be shown later, to obtain the solutions over a period $[0,2\pi]$, we need only calculate those in $[0,\pi]$, from which the solution in $[\pi,2\pi]$ can be inferred; this property would lead to significant savings on the computational cost. Moreover, according to (2.16), we conclude that μ and $\widetilde{\mu}$ are simultaneous eigenvalues, indicating physically the possibility of existence of left and right propagating waves with the same growth rate and behaviours of motion. Finally, we notice that the symmetry property discussed is due to the relation of the basic velocity profile

$$U(y,t+\pi) = -U(y,t), \tag{2.18}$$

which also exists for other periodic flows with zero mean, such as the oscillatory plane Stokes layers in which a similar symmetry property has been revealed (e.g. von Kerczek & Davis 1974; Blennerhassett & Bassom 2002; Gao & Lu 2006*b*).

3. Numerical procedure

To obtain the finite-wavelength solutions, the governing equation (2.7) subject to the boundary conditions (2.8) to (2.12) is solved using a Chebyshev spectral collocation technique. The continuous function ϕ is discretized on the Gauss–Lobatto collocation points on the interval $-1 \leqslant y \leqslant 0$ such that

$$\phi_j(t) = \phi(y_j,t), \quad y_j = \frac{1}{2}\left(\cos\frac{j\pi}{N} - 1\right), \quad j = 0,1,\ldots,N. \tag{3.1}$$

Since the time-dependent Orr–Sommerfeld equation (2.7) should be satisfied at these collocation points, we then obtain a set of ordinary differential equations in time, which are symbolically written as

$$2\beta^2 \boldsymbol{L}\frac{\mathrm{d}\boldsymbol{\phi}}{\mathrm{d}t} + \mathrm{i}kR\boldsymbol{M}(t)\boldsymbol{\phi} = \boldsymbol{S}\boldsymbol{\phi}, \tag{3.2}$$

where $\boldsymbol{\phi} = (\phi_0,\phi_1,\ldots,\phi_N)^T$ is the approximation of the function ϕ; the time-independent square matrices $\boldsymbol{L}$ and $\boldsymbol{S}$ represent the continuous operators, i.e.

$$\frac{\partial^2}{\partial y^2} - k^2 \to \boldsymbol{L}, \quad \frac{\partial^4}{\partial y^4} - 2k^2\frac{\partial^2}{\partial y^2} + k^4 \to \boldsymbol{S}, \tag{3.3}$$

and can be straightforwardly created using the Differentiation Matrix Suite by Weideman & Reddy (2000); the time-dependent matrix

$$\boldsymbol{M}(t) = \boldsymbol{U}(t)\boldsymbol{L} - \boldsymbol{U}_{yy}(t), \tag{3.4}$$

with $\boldsymbol{U}$ and $\boldsymbol{U}_{yy}$ denoting the diagonal matrices with the elements of the mesh values of U and U_{yy}, respectively. The discretized approximation of the boundary conditions can be obtained in a similar way.

The boundary conditions should be treated more carefully and are enforced in an explicit way by adding additional equations to the main system (3.2) (Canuto *et al.*

1988; Fornberg 1996; Weideman & Reddy 2000). Since (3.2) includes $N+1$ equations, together with six boundary conditions, we have in total $N+7$ equations to determine the unknown eigenvector $\boldsymbol{\varphi} = (\phi_0, \phi_1, \ldots, \phi_N, h, \xi)^T$ comprised of $N+3$ variables. To make the numbers of the equations and unknowns consistent, we omit four equations of (3.2) evaluated at the exterior points $y_j (j = 0, 1, N-1, N)$. Then the remaining equations and boundary conditions can be combined to give

$$\boldsymbol{B}\frac{\mathrm{d}\boldsymbol{\varphi}}{\mathrm{d}t} = \boldsymbol{A}(t)\boldsymbol{\varphi}, \tag{3.5}$$

where $\boldsymbol{A}(t)$ is a 2π-periodic coefficient matrix, and $\boldsymbol{B}$ is a constant matrix of appropriate size. Owing to the absence of temporal derivatives in the boundary conditions at the wall (2.8) and the tangential tress condition (2.10), $\boldsymbol{B}$ has a singular behaviour, and hence the system (3.5) cannot be integrated directly. This difficulty can be overcome by expressing ϕ_0, ϕ_{N-1} and ϕ_N in terms of other ϕ_j as well as h and ξ based on the discretized forms of (2.8) and (2.10).

Following the Floquet theory, the fundamental matrix solution of (3.5), $\boldsymbol{\Phi}$, has the form

$$\boldsymbol{\Phi}(t) = \boldsymbol{P}(t)\mathrm{e}^{t\boldsymbol{Q}}, \tag{3.6}$$

where the matrix $\boldsymbol{P}$ is 2π-periodic in t, and the eigenvalues of the matrix $\boldsymbol{Q}$ are just the Floquet exponents μ_j. Without any loss of generality, the initial value of $\boldsymbol{\Phi}$ can be taken as the appropriately sized identity matrix, i.e.

$$\boldsymbol{\Phi}(0) = \boldsymbol{I}. \tag{3.7}$$

It is easy to prove that

$$\boldsymbol{\Phi}(2\pi) = \mathrm{e}^{2\pi\boldsymbol{Q}}. \tag{3.8}$$

Let λ_j denote the eigenvalues of $\boldsymbol{\Phi}(2\pi)$, then the Floquet exponents μ_j are related to λ_j by

$$\mu_j = \frac{1}{2\pi}\ln\lambda_j. \tag{3.9}$$

The system (3.5) is integrated in time using the fourth-order Runge–Kutta method with the initial condition (3.7) to obtain $\boldsymbol{\Phi}(2\pi)$. Note that the treatment of the dependence on time in the present numerical method is different from that used by Or (1997), who expanded the periodic eigenfunctions into Fourier series and obtained an augmented matrix eigensystem which was solved by an iteration method. This procedure is suitable because the instability of the flow in Or (1997) is due solely to the surface deformation, and hence only one eigenvalue need be located. However, as indicated by Gao & Lu (2006*a*) for the long-wavelength analysis, two modes are responsible for the instability when the surfactants are present. The implementation of the numerical time integration of the governing system allows an efficient calculation of all eigenvalues to identify the most unstable mode.

In the present problem, the symmetry property discussed in § 2 can be used to simplify our numerical treatment. We introduce a new matrix $\boldsymbol{\Phi}_c(t)$ as

$$\boldsymbol{\Phi}_c(t) \equiv \boldsymbol{I}_c\boldsymbol{\Phi}(t), \tag{3.10}$$

where $\boldsymbol{I}_c$ is the identity matrix with the signs of the last two elements reversed. $\boldsymbol{\Phi}_c$ may in fact be produced from $\boldsymbol{\Phi}$ under the elementary operation that the last two rows of $\boldsymbol{\Phi}$, associated with the surface deformation h and the surfactant concentration ξ, are

multiplied by -1. Define another matrix $\boldsymbol{\Phi}_1(t)$ such that

$$\boldsymbol{\Phi}_1(t) \equiv \boldsymbol{\Phi}(t)\boldsymbol{\Phi}^{-1}(\pi)\boldsymbol{I}_c, \tag{3.11}$$

which is also a fundamental matrix of (3.5) because of the homogeneous behaviour of the system. It follows that

$$\boldsymbol{\Phi}_1(\pi) = \boldsymbol{I}_c = \widetilde{\boldsymbol{\Phi}}_c(0), \tag{3.12}$$

and hence we have

$$\boldsymbol{\Phi}_1(t) = \widetilde{\boldsymbol{\Phi}}_c(t-\pi) \tag{3.13}$$

in view of the symmetry property. Therefore

$$\boldsymbol{\Phi}_1(2\pi) = \widetilde{\boldsymbol{\Phi}}_c(\pi). \tag{3.14}$$

Finally, according to (3.11) and using $\boldsymbol{I}_c^{-1} = \boldsymbol{I}_c$, we obtain

$$\boldsymbol{\Phi}(2\pi) = \boldsymbol{\Phi}_1(2\pi)[\boldsymbol{\Phi}^{-1}(\pi)\boldsymbol{I}_c]^{-1} = \boldsymbol{\Phi}_1(2\pi)\boldsymbol{I}_c\boldsymbol{\Phi}(\pi) = \widetilde{\boldsymbol{\Phi}}_c(\pi)\boldsymbol{\Phi}_c(\pi). \tag{3.15}$$

Since the value of $\boldsymbol{\Phi}(2\pi)$ can be calculated from $\boldsymbol{\Phi}(\pi)$, the system (3.5) can be integrated only over the interval $0 \leqslant t \leqslant \pi$, and hence the overall computational cost is halved. The symmetry property (3.15) has been verified by our numerical results, and can in turn serve as a verification of our spectral code. Similar characteristics have also been derived by von Kerczek & Davis (1974) on the stability of a Stokes layer in a channel and by Gao & Lu (2006*c*) on the stability of the plane Poiseuille flow with an oscillatory wall suction/blowing, wherein an inherent temporal or spacial symmetry property is exhibited in the basic velocity profile.

The number of Chebyshev points N in the present calculations is increased until the Floquet exponents μ obtained are accurate to at least four significant figures. In general, a larger N is needed for higher R and k, while it has been shown that the accuracy of the results is not sensitive to the number of time steps over a half period, K, provided that K is large enough to maintain the stability of numerical procedure. Typically, $20 \leqslant N \leqslant 50$ and $200 \leqslant K \leqslant 1000$ have been taken to determine the neutral curves and the critical conditions for various parametric regimes. All the calculations are performed in Matlab.

In addition to the internal self-consistency of the numerical procedure due to the symmetry property of the problem, the accuracy of the current results has been further confirmed by comparing the numerical results with the analytical solutions in the limit of long-wavelength disturbances. According to Gao & Lu (2006*a*), for $k \ll 1$, the eigenvalues dominating the stability of the flow can be approximated as $\mu \approx \theta R^2 k^2 / 2\beta^2$, where θ satisfies a quadratic equation. Figure 2 shows the variation of μ, corresponding to the first two eigenvalues of the most dangerous mode, as a function of k for $R = 200$, $\chi = 0$, $M = 10^{-3}$ and $\beta = 2$ or 3. For $\beta = 2$, both the eigenvalues are real and positive (figure 2*a*), and hence the corresponding modes are unstable. For $\beta = 3$, the eigenvalues are complex conjugate to each other and only the eigenvalue with positive imaginary part is shown in figure 2(*b*). Since the growth rates $\mu_r < 0$, the long-wave modes are damped and $-\mu_r$ is used as the vertical ordinate in a logarithmic scale for clear demonstration. Excellent agreement between the present numerical results and theoretical predictions, especially for $k < 10^{-2}$, can be observed. Further verification of the numerical results will be shown in the following section.

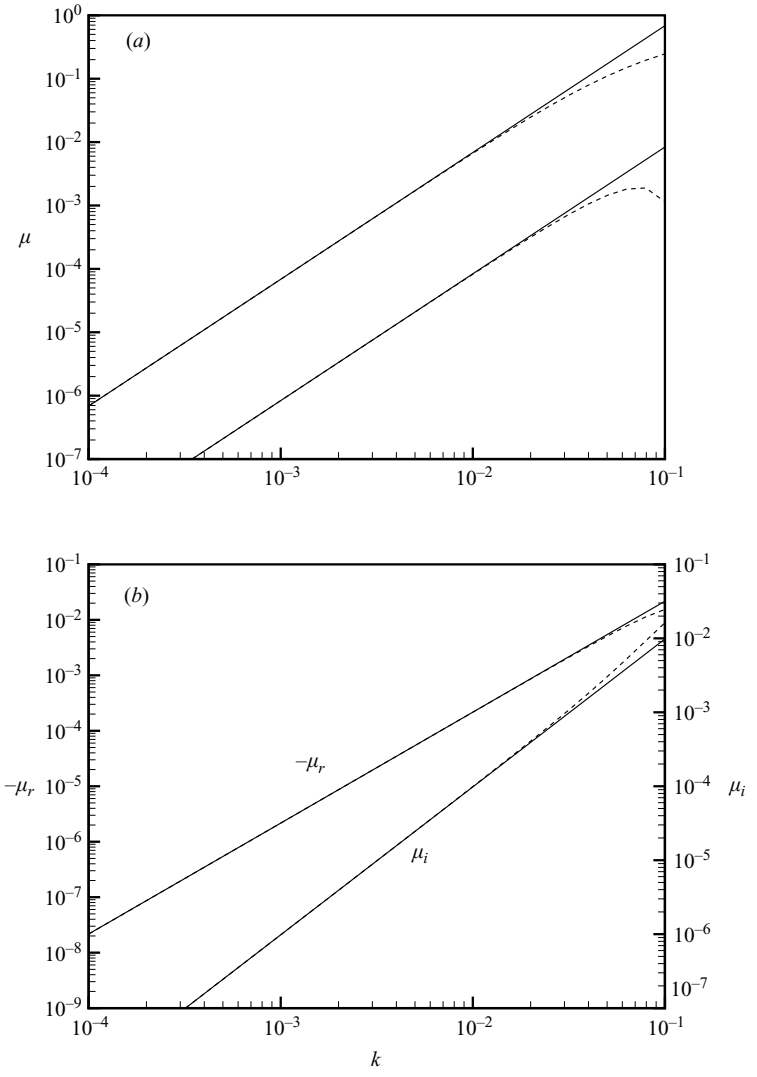

FIGURE 2. Comparison of the numerical results (dashed line) for arbitrary wavenumbers with the analytical results (solid line) of Gao & Lu (2006*a*) for long waves at $R = 200$, $\chi = 0$ and $M = 10^{-3}$. The first two eigenvalues are (*a*) real for $\beta = 2$ and (*b*) complex conjugate for $\beta = 3$.

4. Results and discussion

Since the Floquet exponents μ are dependent on six parameters, as in (2.17), it is difficult to study the stability characteristics of the oscillatory film flow in the whole parameter space. In the present study, we mainly investigate the combined effects of the modulation and the surfactant, and thus set the parameters as fixing χ and ψ and varying β, R and M. In accordance with Or (1997), we choose $\psi = 0.05$. Depending on whether or not gravity is involved, the dimensionless number χ is specified to be $\chi = 0$ or $\chi = 1$. As indicated by Gao & Lu (2006*a*) for the long-wave analysis, the stability characteristics of the flow without gravity may be quite different from those with gravity, and hence the corresponding results are shown separately. Here,

we mainly discuss the results in the absence of gravity, which have been mentioned less in the previous work but are of great importance (Ostrach 1982), and briefly on the results in the presence of gravity.

4.1. *Clean surface in the absence of gravity*

When gravity is absent, i.e. $\chi = 0$, the long-wavelength instability of the flow depends only on β and M, and the neutral curves have been analysed by Gao & Lu (2006*a*). For $0 < \beta < 10$, there exist three unstable intervals of β alternating with three regions on which the flow is stable subject to long-wavelength perturbations. The edges of these intervals are dependent on M and remain unchanged for sufficiently large values of M. However, over the stable intervals, finite-wavelength instability may occur when the Reynolds number R exceeds a critical value R_c as shown below, even though the long-wavelength perturbations are damped.

For finite-wavelength instabilities, we begin with the analysis of the oscillatory fluid layer in the absence of surfactant. The variation of the critical Reynolds number R_c for the stability of a clean surface in the presence of gravity ($\chi = 1$) has been given by Or (1997), where a parameter $R/\chi^{1/2}$ is used as the ordinate, and is only different from the Froude number F in (2.14) by a factor of $\sqrt{2}$. Obviously, the parameter is inapplicable for $\chi = 0$, and the critical Reynolds number for the zero-gravity case cannot be inferred from the results in Or (1997). Instead, we use the Reynolds number R as the ordinate to present our results.

Figure 3 shows the stability boundaries for $\chi = M = 0$ and $\psi = 0.05$. In figure 3(*a*), the long-wave boundaries of Yih (1968) are represented by the vertical dotted lines, which divide the β-axis into alternate stable and unstable intervals, denoted by S and U, respectively, in the sense of long-wave perturbations. Over the unstable intervals, the flow is unstable for any non-zero Reynolds number. As β increases from the long-wave unstable intervals to the stable ones, three oblique curves, corresponding to the finite-wavelength stability boundaries, branch off from the long-wave straight lines at the points P_1, P_2 and P_3. The wavenumbers of the disturbances associated with the finite-wavelength instability are shown in figure 3(*b*). Along each finite-k curve, an increase of β leads to an approximately exponential increase of the Reynolds number. The corresponding wavenumber k increases monotonically along the first and third curves, and a careful examination of the second curve exhibits a slightly non-monotonic behaviour with a local minimum at $\beta = 6.5$ approximately. When β crosses the vertical lines at the right-hand edge of each long-wave stable interval, the long-wave disturbances become the physically preferred ones again, though the finite-wave instability may also occur for sufficiently large R above the dashed curves. Owing to the competition of the long-wave instability and the finite-wavelength instability at relatively lower wavernumbers, only the solid-line portions of the finite-k curves in figure 3 represent the critical Reynolds number R_c and the corresponding critical wavenumber k_c. Thus, for the parameters lying in the regions denoted by S in figure 3(*a*), the flows are stable for both the long- and finite-wavelength perturbations. It is necessary to indicate that the neutral modes dominating the stability of the oscillatory clean surface are always associated with zero eigenvalues, i.e. $\mu_r = \mu_i = 0$, and therefore have the form of standing waves.

Different behaviours of the stability characteristics at the branch points can be identified in figure 3(*a*). The critical wavenumber k_c increases continuously from zero around P_1 and P_3; while near P_2, the long-wave instability switches to the finite-wave type in a discontinuous way so that the corresponding curve in figure 3(*b*) starts from a finite value of k_c, which should be determined numerically. To discuss why

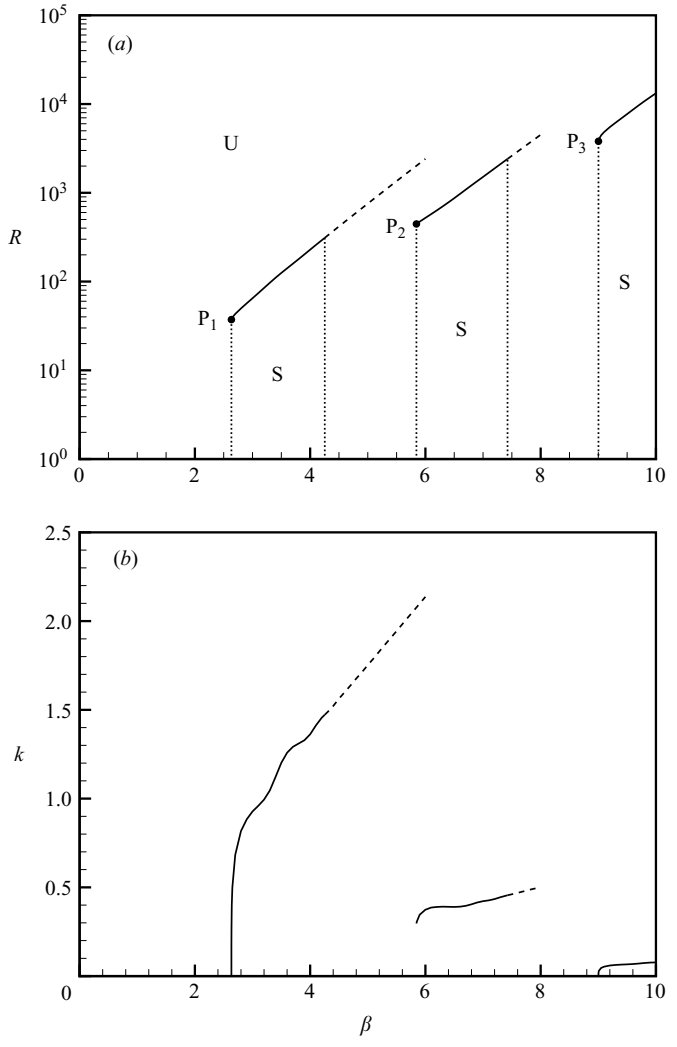

FIGURE 3. Stability characteristics in the absence of surfactants for $\chi = 0$, $M = 0$ and $\psi = 0.05$. (a) Stability boundaries in the (β, R)-plane. The long-wave boundaries of Yih (1968) are denoted by the vertical dotted lines; the finite-wavelength boundaries are denoted by the oblique lines. The solid-line portions represent the variation of the critical Reynolds number R_c, while the dashed-line portions do not represent criticality owing to the competition of long waves. The three branch points are indicated by P_1, P_3 and P_3. Stable and unstable regions are denoted by S and U, respectively. (b) Variation of the corresponding wavenumber k with β.

such a difference occurs, typical neutral curves in the (k, R)-plane for the values of β near P_1 and P_2 are plotted in figure 4. The neutral curves near P_3 are qualitatively similar to those near the first one except for much higher R, and are not exhibited here. As shown in figure 4, even a small increase of β can cause significant variations of the structures of the neutral curves in the long-wavelength region, while only a relatively weak influence of β in the finite-wavelength region is observed. For $\beta = 2.63380$ in figure 4(a), the neutral curve increases monotonically as k increases. Since the long-wave instability occurs for all non-zero values of R, the neutral curve starts from the origin which is outside the scale of the figure. The upper dashed

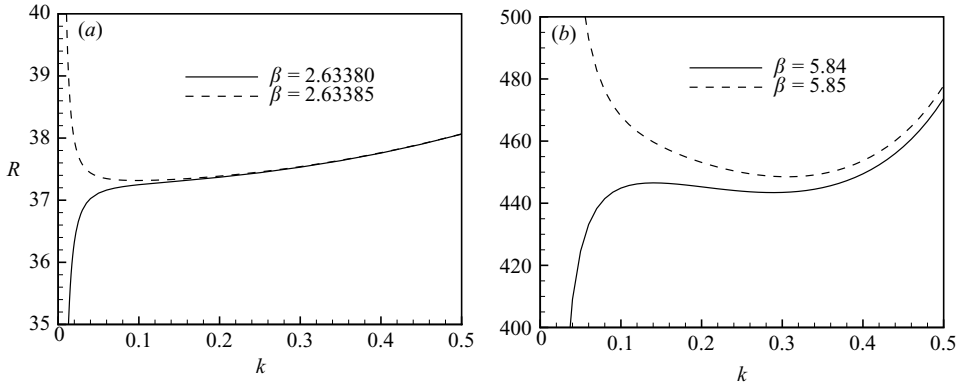

FIGURE 4. Neutral curves in the (k, R)-plane for typical values of β close to (a) the first branch point P_1 and (b) the second branch point P_2 in figure 3.

neutral curve, corresponding to $\beta = 2.63385$, has a minimum at $k_c = 0.098$ and hence a finite-wavelength instability occurs. Note that near the first branch point P_1, the variation of the critical wavenumber k_c is very sensitive to β. As β decreases to the first long-wave boundary at $\beta = 2.63383$, k_c approaches zero very steeply (figure 3*b*). The neutral curves near the second branch point P_2 at $\beta = 5.844$ are plotted in figure 4(*b*) and exhibit some different features. The solid neutral curve for $\beta = 5.84$ has a local minimum at $k = 0.29$ approximately. However, this minimum is not related to criticality owing to the competition of the long-wave instability. Once β increases to 5.85, the long-wave instability is eliminated and the critical point associated with the finite-wavelength instability is close to the local minimum of the solid curve, leading to a jump of the critical wavenumber from zero to a finite value $k_c \approx 0.30$ at P_2 in figure 3(*b*).

4.2. *Effect of surfactants in the absence of gravity*

To exhibit an overview of the stability characteristics of an oscillatory fluid layer covered by the surfactants, we first present some results at a typical value $M = 10^{-3}$ with the other parameters being the same as those in figure 3. Figures 5(*a*) and 5(*b*) show the stability boundaries in the (R, β)-plane and the corresponding wavenumbers of the neutral modes, respectively. The long-wave boundaries are also exhibited by the vertical dotted lines. Note that the width of each unstable interval for the long-wave modes is narrowed owing to the presence of the surfactant. As β increases to the left-most vertical line, the first branch curve for the finite-wavelength instability emerges. The relevant wavenumber k, which is now also the critical wavenumber k_c, increases rapidly from zero to a local maximum 0.9 approximately at $\beta \approx 3$. Further increase of β will shift the instability to the long-wave region once more. Different from the clean-surface case, along this branch curve, there exist two modes which belong to two complex-conjugate eigenvalues with $\mu_i \neq 0$. Thus, the neutral modes have the form of travelling waves. Meanwhile, another finite-wavelength stability boundary with higher wavenumbers can be identified. Detailed examination of this stability boundary exhibits zero eigenvalues, and hence standing-wave modes are preferred, similar to the clean-surface case. Line-crossing of the two finite-wavelength instability boundaries occurs at $\beta = 3.15$, as denoted by the point P, above which the standing-wave modes are responsible for the onset of the instability until the long-wave instability takes over at $\beta = 4.71$. However, the second finite-wavelength stability

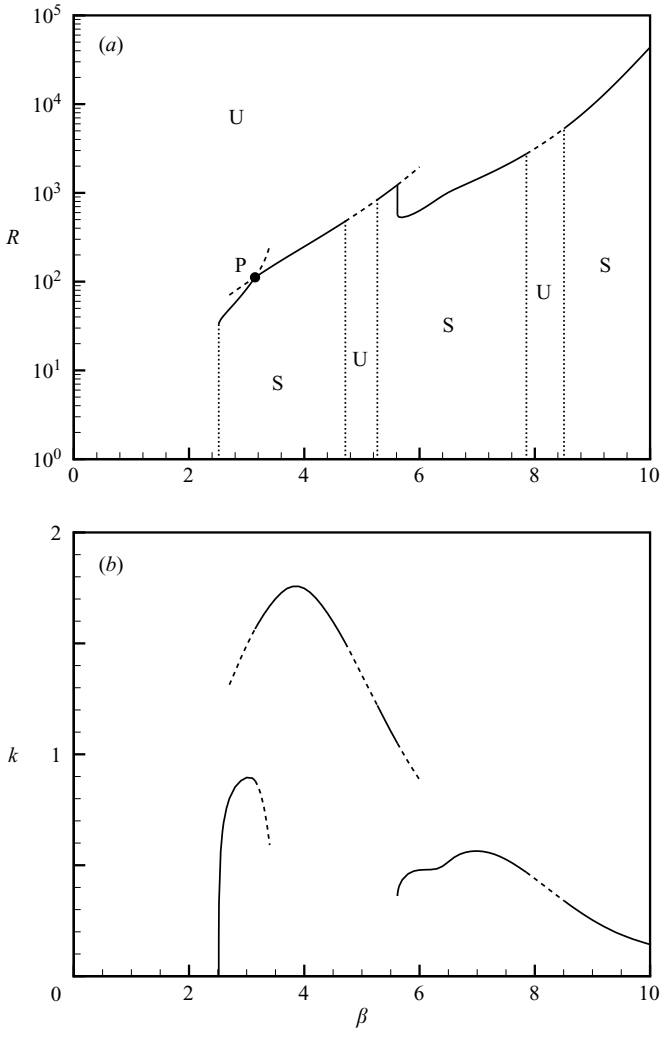

FIGURE 5. Stability characteristics in the presence of surfactants for $\chi = 0$, $M = 10^{-3}$ and $\psi = 0.05$. (*a*) Stability boundaries in the (β, R)-plane. The long-wave boundaries of Gao & Lu (2006*a*) are denoted by the vertical dotted lines; the finite-wavelength boundaries are denoted by the oblique lines. The solid-line portions represent the variation of the critical Reynolds number R_c, while the dashed-line portions do not represent criticality owing to the competition of long waves. Stable and unstable regions are denoted by S and U, respectively. (*b*) Variation of the corresponding wavenumber k with β.

boundary persists even on the interval $5.27 < \beta < 7.85$, corresponding to the second stable range for the long-wave modes. Figure 5(*b*) shows that the wavenumbers vary with β in an obviously non-monotonic way, compared with figure 3(*b*). Another finite-wavelength stability boundary emanating from a point at $\beta \approx 5.62$ begins to dominate the stability for higher values of β, except over the third long-wave unstable interval $7.85 < \beta < 8.51$. The occurrence of this stability boundary is due to the emergence of an isolated unstable island in the (k, R)-plane, which expands as β increases. Similar behaviour has also been addressed by Or (1997) in detail. We notice that this stability boundary is also associated with standing-wave modes. Unlike the clean-surface case,

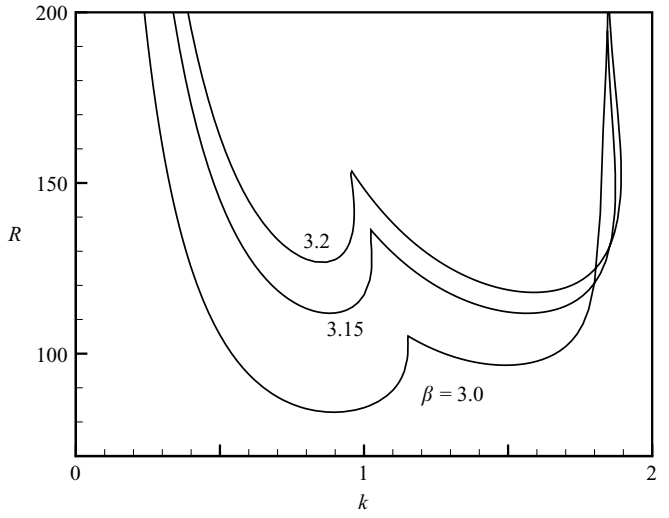

FIGURE 6. Typical neutral curves in the (k, R)-plane for $M = 10^{-3}$, $\chi = 0$, $\psi = 0.05$ and values of β around the intersection point P in figure 5. The left-hand portion of each curve is associated with travelling-wave modes, and the right-hand portion with standing-wave modes.

no finite-wavelength curves branching from the long-wave boundary of the second and third stable interval are detected.

Typical neutral curves in the (k, R)-plane for $M = 10^{-3}$, $\chi = 0$ and $\psi = 0.05$ are shown in figure 6. The values of β are taken to be 3.0, 3.15 and 3.2, with the curve for $\beta = 3.15$ corresponding to the intersection point of the stability boundaries in figure 5, denoted by P. It is seen that each neutral curve can be divided into two portions, and each portion has a minimum. For $\beta = 3.0$, the left-hand minimum is lower than the right-hand one and thus the instability is dominated by the low-wavenumber mode with the critical value $R_c = 82.8$ and $k_c = 0.895$. As β increases, the neutral curve shifts upwards, and the left-hand portion moves more rapidly than the right-hand one. For $\beta = 3.15$, both minima represent criticality, which is related to the onset value of the Reynolds number $R_c = 112$ and two critical wavenumbers $k_c = 0.88$ and 1.56. As β increases to 3.2, the right-hand minimum eventually is responsible for the criticality with $R_c = 117.9$ and $k_c = 1.59$. This leads to a non-continuous variation of the critical wavenumber, as exhibited by the solid lines in figure 5(b), while the variation of the critical Reynolds number is still continuous. A similar jump of the wavenumber has also been observed by Phillips (2001).

Further, the numerical results show that the left-hand portion of the curve in figure 6 is connected to complex-conjugate eigenvalues while the right-hand portion is connected to zero eigenvalues. This behaviour can be inferred from figure 7, in which the growth rates, μ_r, of the first four Floquet modes are presented as a function of R for $\beta = 3.0$. The wavenumber k is specified to be 1 and 1.5, corresponding to the left- and right-hand portions of the thick neutral curve in figure 6, respectively. The solid curves represent purely real eigenvalues relevant to the standing-wave disturbance modes, and the dashed curves denote the real parts of two complex-conjugate eigenvalues relevant to the travelling-wave modes. Two complex-conjugate eigenvalues bifurcate on the real axis at the left-hand endpoint of each dashed line, and coalesce on the real axis again at the right-hand endpoint. Similar interactions of the real and complex eigenvalues have also been found by Blennerhassett & Bassom

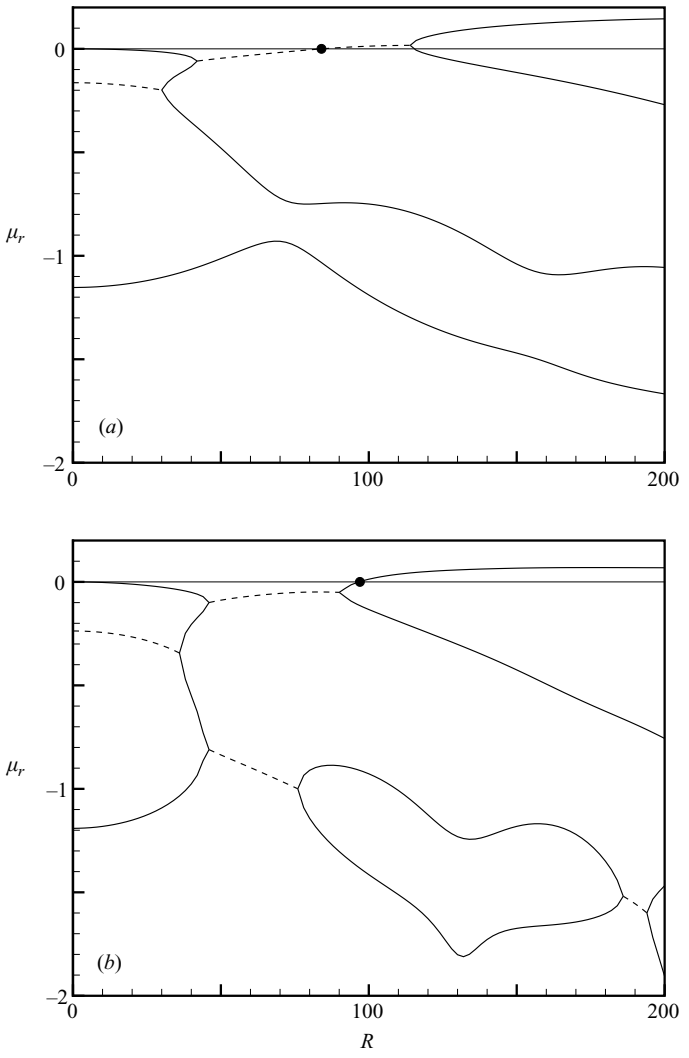

FIGURE 7. Variation of the real part of μ, μ_r, corresponding to the first four modes as a function of R for $\chi = 0$, $\psi = 0.05$, $M = 10^{-3}$, $\beta = 3.0$ and (*a*) $k = 1$, (*b*) $k = 1.5$. The solid curves represent purely real values of μ related to standing waves, and the dashed curves denote two complex μ related to travelling waves. The solid circles denote where neutral modes responsible for criticality occur.

(2006) for the stability of an oscillatory flow in a wide channel. At low values of R, the solid curve of the first real eigenvalue is very close to but still less than zero and corresponds to damped disturbance modes. The values of μ in the limit of $R \to 0$ can be obtained asymptotically and are given in the Appendix. As an additional verification of our code, three eigenvalues obtained by the low-R asymptotics and numerical calculations are given in table 1 for comparison. The first eigenvalue is zero, corresponding to only the trivial solution. The second and third eigenvalues are complex conjugate and the fourth is real. The numerical results calculated for $R = 0.5$ are accurate to four significant figures at least. Calculations performed at sufficient small values of R produce the full precision and the relevant results are not

		Complex μ	Real μ
$k=1$	A	$(-0.163600, \pm 0.129833)$	$(-1.153222, 0)$
	N	$(-0.163610, \pm 0.129819)$	$(-1.153209, 0)$
$k=1.5$	A	$(-0.237132, \pm 0.347132)$	$(-1.190857, 0)$
	N	$(-0.237149, \pm 0.347087)$	$(-1.190834, 0)$

TABLE 1. Comparison of the Floquet exponents μ for $R \to 0$, $k=1$ and 1.5 obtained by asymptotic predictions (A) and numerical calculations (N). Numerical results are calculated at $R=0.5$. Other parameters are the same as those in figure 7.

shown here. For $k=1$ in figure 7(a), the neutral mode in the form of a travelling wave is first encountered at $R=84.2$, where a dashed curve passes through zero, as indicated by the solid circle. For $k=1.5$ in figure 7(b), a zero eigenvalue is obtained at $R=98.4$, corresponding to the neutral mode in the form of a standing wave. Here, it is necessary to note that the first two modes, responsible for the instability, are coupled with each other. This behaviour is different from the stability of steady film flow (e.g. Blyth & Pozrikidis 2004*a*; Wei 2005*a*), in which the modes can be easily distinguished and are usually named the interface mode (or Yih mode) and the surfactant mode (or Marangoni mode).

To investigate whether the flow is stabilized or destabilized by the presence of surfactant, extensive calculations of the critical Reynolds number R_c and the relevant critical wavenumber k_c have been performed for a variety of M and β. When M varies, three families of the finite-wavelength stability boundaries, lying in the three long-wave stable ranges of the modulation frequency, respectively, are obtained. Here, we will study each family separately. Stability characteristics of the flow over the first, second and third long-wave unstable intervals, corresponding to low-, medium- and high-frequency ranges of modulation, respectively, are shown in figures 8 to 10.

Figure 8(a) shows the variation of the critical Reynolds number, R_c, as a function of β in the low-frequency range for several values of M. To exhibit clearly the differences among the curves, the stability boundaries are also plotted in figure 8(b) using $\mathrm{e}^{-\beta}R_c$ as an ordinate. The endpoints of each curve correspond to the long-wave boundaries. For neatness, the vertical lines relevant to the long-wave boundaries and the finite-wavelength boundaries not associated with criticality are not drawn here. The surfactant affects the stability characteristics of the flow in the following ways. First, the increase of surface elasticity broadens the stable range of β for the long-wave perturbation modes, that has been discussed in Gao & Lu (2006*a*). Secondly, the disturbances in the form of travelling waves may dominate the instability, different from the clean-surface case. Thirdly, the surfactant may have a stabilizing (destabilizing) influence on the flow by raising (lowering) the critical Reynolds number R_c for the onset of instability. For $M=10^{-5}$, corresponding to a weak surface elasticity, R_c and k_c are only slightly modified and a stabilizing influence can be observed. The relevant critical modes are the travelling waves, as indicated by the non-zero μ_i in figure 8(d). As M increases, the stability boundary in figure 8(a, b) begins to consist of the left-hand travelling-wave portion and the right-hand standing-wave portion, as described above. The travelling-wave portion becomes shorter with increasing M and eventually disappears for $M=10^{-1}$. In addition, the critical Reynolds numbers of the travelling-wave portions are always higher than those of the clean-surface case. The standing-wave portion moves downwards as M increases and may intersect with

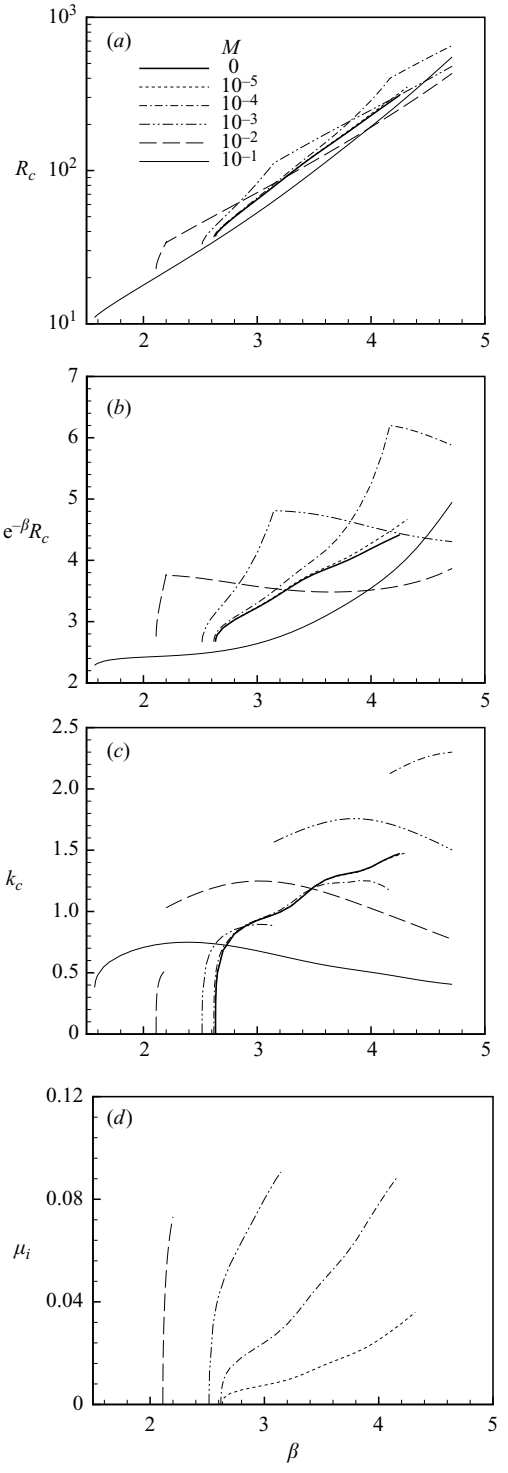

FIGURE 8. Effects of surfactants on the stability characteristics of the flow in the low-frequency range. Variation of (*a*) the critical Reynolds number R_c, (*b*) $\mathrm{e}^{-\beta}R_c$, (*c*) the critical wavenumber k_c and (*d*) the imaginary part of μ, μ_i, at criticality as functions of β for various values of M. The endpoints of each curve correspond to the long-wave boundaries.

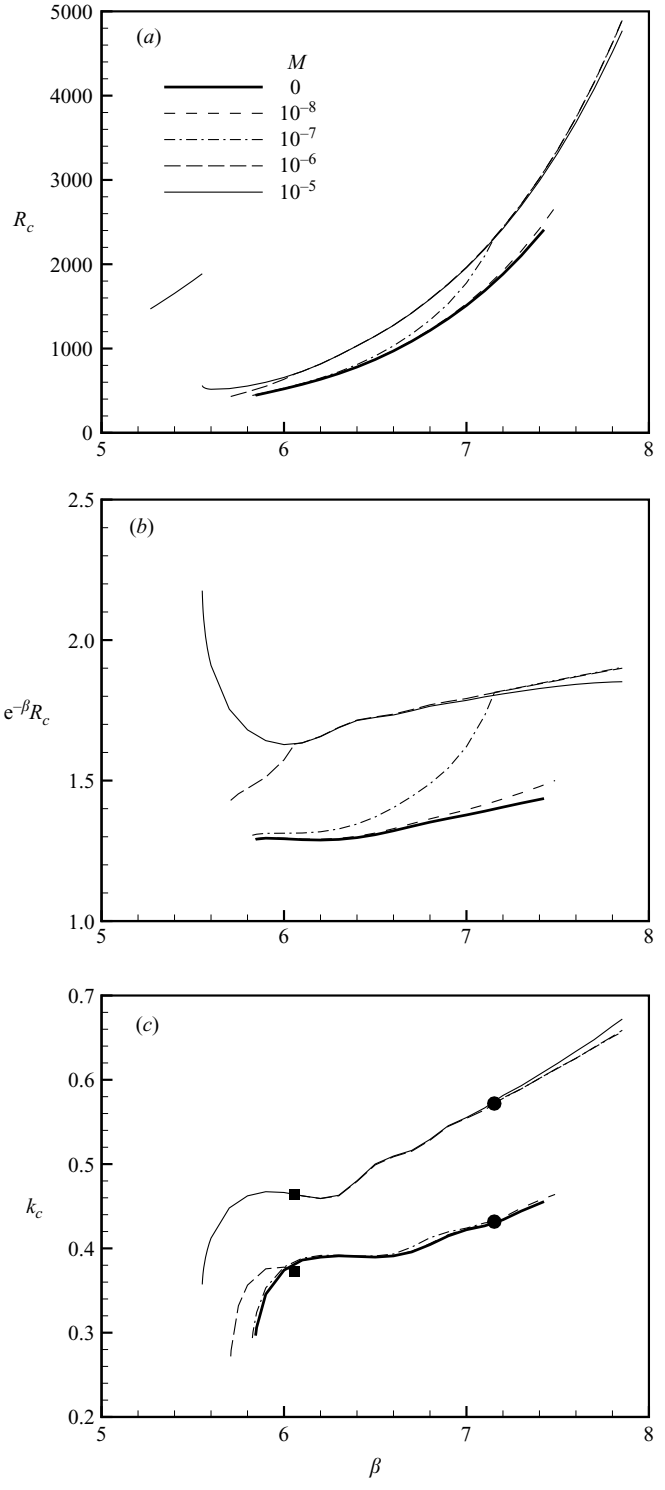

FIGURE 9. Variation of (*a*) R_c, (*b*) $\mathrm{e}^{-\beta}R_c$ and (*c*) k_c as functions of β in the medium-frequency range, where the solid circle and square represent the discontinuity locations of the curves for $M = 10^{-7}$ and 10^{-6}, respectively.

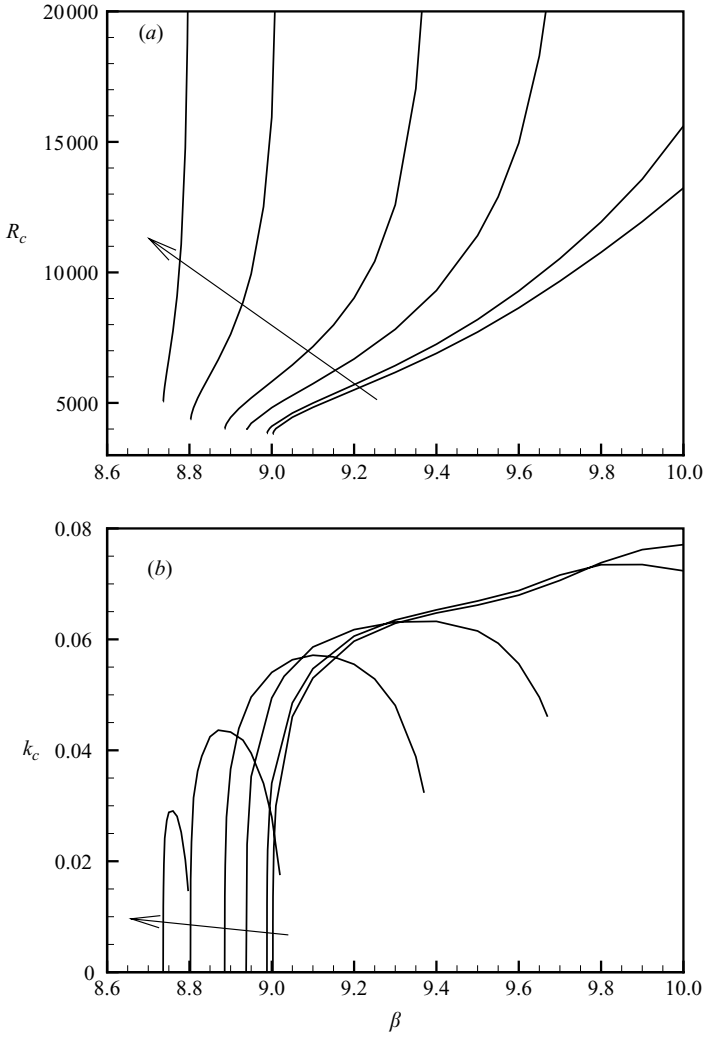

FIGURE 10. Variation of (*a*) R_c and (*b*) k_c as functions of β in the high-frequency range. The arrows indicate the direction of increasing M: $M = 0$, 1×10^{-10}, 5×10^{-10}, 1×10^{-9}, 2×10^{-9} and 3×10^{-9}.

the thick solid curve related to the clean-surface case. Thus, the flow is stabilized on the left-hand side of the intersecting point and destabilized on the right-hand side. For $M = 10^{-1}$, the critical curve lies underneath the thick solid curve, so that the finite-wavelength instability of the clean-surface is always enhanced. For sufficiently large M, the change of the instability from the long- to finite-wavelength type occurs in a discontinuous way, which can be explained by the neutral curves similar to figure 4. Here, we should emphasize that the destabilizing effects of insoluble surfactants in the sense of lowering the critical Reynolds number is a new finding. The destabilization of the surfactants has never been found on the stability of the flow in the framework of long-wave theory (Gao & Lu 2006*a*) as well as the stabilities of other configurations of free-surface flow without surface shear (e.g. Whitaker& Jones 1966; Lin 1970; Blyth & Pozrikidis 2004*a*), in which only stabilizing effects of the surfactants have been found.

The finite-wavelength stability boundaries in the second family are shown in figure 9, corresponding to the medium range of the modulation frequency. Compared with the low-frequency range, much higher values of R_c are encountered. Since $M = Ma/\psi R^2$ and the physically preferred values of the Marangoni number Ma are of $O(1)$, we have much smaller values of M. A common feature of these curves is that the critical wavenumber k_c does not tend to zero near the long-wave boundary. The curve for $M = 10^{-8}$ corresponds to the critical modes in the form of travelling waves. Both the travelling-wave and standing-wave instabilities occur for $M = 10^{-7}$ and 10^{-6}, as described above. In figure 9(a), a discontinuous behaviour can be observed on the stability boundary for $M = 10^{-5}$, whose left-hand portion actually belongs to the first family of stability boundaries in figure 8 (see also figure 5), and the corresponding curves are outside the scales in figures 9(b) and 9(c). The increase of M leads mainly to the decrease of the frequency, at which the curves are split into two portions related to different stability features. The critical Reynolds number R_c and critical wavenumber k_c on the right-hand portions are insensitive to the variation of surfactant elasticity, and the curves for various M can hardly be distinguished. To show clearly the results in figure 9(c), we use the solid circles and squares to mark the discontinuity locations of the curves for $M = 10^{-7}$ and 10^{-6}, respectively. Thus, the curves on the left (right) of the symbols represent the critical wavenumbers for travelling (standing) waves. It is seen in figure 9(a) that the curves for the surfactant-covered surface lie above the clean-surface curve, and hence the sufactants play a stabilizing role in the flow for the parameters considered here. However, the flow may also be destabilized for sufficiently large values of M, e.g. $M = 10^{-3}$ in figure 5.

Figure 10 shows the variation of the critical Reynolds number R_c and wavenumber k_c versus β in the high-frequency range. Detailed examination of the neutral curves in the (k, R)-plane shows the existence of two unstable regions; one is related to the travelling-wave instability at small wavenumbers and the other to the second family of stability boundaries at large wavenumbers. Here, we deal mainly with the travelling-wave instabilities which are dominant for the parameters considered. Figure 10(b) shows that the critical wavenumber exhibits a non-monotonic behaviour. The critical Reynolds number increases when the surfactant is introduced. In addition, the width of the interval of β, where the instabilities of travelling-wave modes occur, shrinks as M increases, and eventually disappears for sufficiently large M. This behaviour reasonably explains why the finite-wavelength boundary branching off the long-wave boundary is not detected for $M = 10^{-3}$ in figure 5.

4.3. *Cases in the presence of gravity*

We now turn to the cases in the presence of gravity with some typical parameters. Figure 11 shows the stability boundaries of a clean surface with $M = 0$ (thin line) and a surfactant-covered surface with $M = 10^{-2}$ (thick line). The parameter χ characterizing the strength of gravity is chosen as 1. Note that the case of $M = 0$ has been studied by Or (1997). We reinvestigate the clean-surface case here to validate our code on the one hand, and to examine Or's results on the other hand. In the absence of surfactant, the finite-wavelength stability boundaries, represented by the oblique curves in figure 11(a), are in excellent agreement with those in Or (1997) except at large values of β, where, as clearly exhibited in figure 11(b), a crossover of the second and third branches occurs, which is different from Or (1997). The difference seems to be due to more strict criteria for the convergence employed in the present calculations. In addition, the wavenumber k relevant to the finite-wavelength instability predicted by Or is exhibited by the circles in figure 11(c) for comparison. There is satisfactory

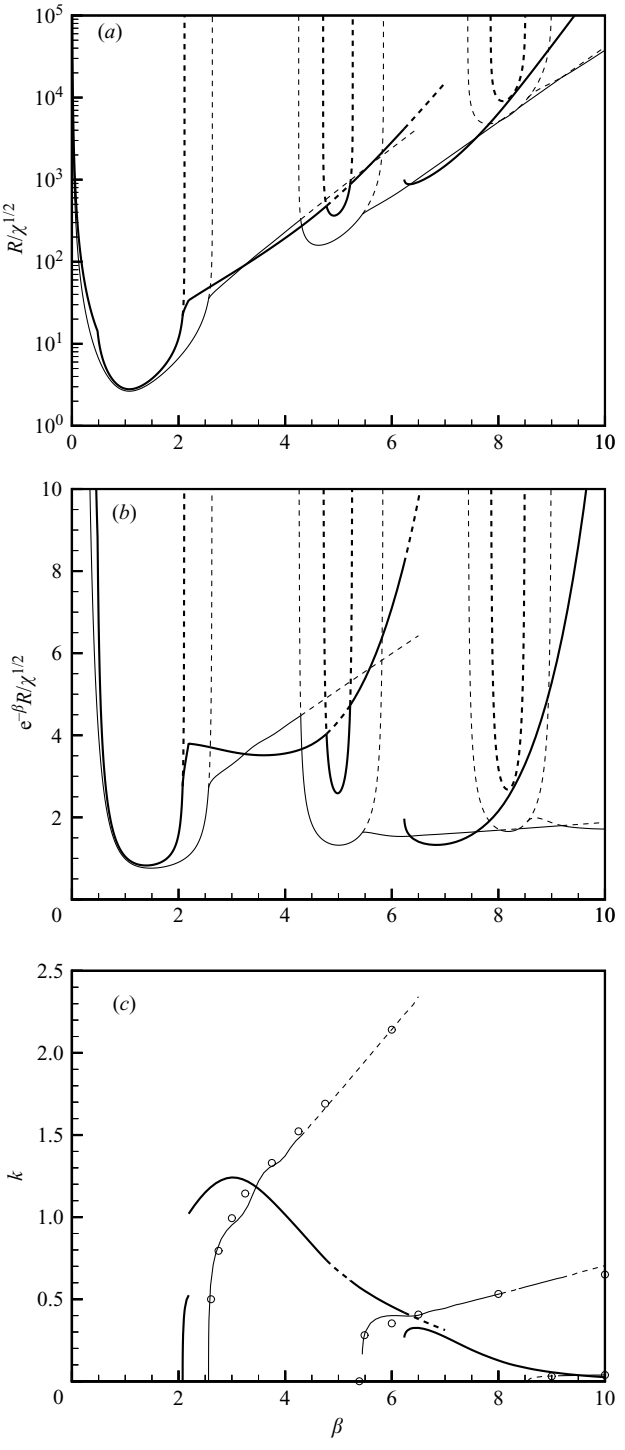

FIGURE 11. Stability boundaries in the (*a*) (β, $R/\chi^{1/2}$)-plane and (*b*) (β, $e^{-\beta}R/\chi^{1/2}$)-plane, and (*c*) variation of the corresponding wavenumber k with β for $\chi = 1$, $\psi = 0.05$, $M = 0$ (thin line) or 10^{-2} (thick line). The solid portions of the curves represent criticality, while the dashed portions are not associated with the critical conditions owing to the competition. Results of Or (1997) are indicated by the circles for comparison.

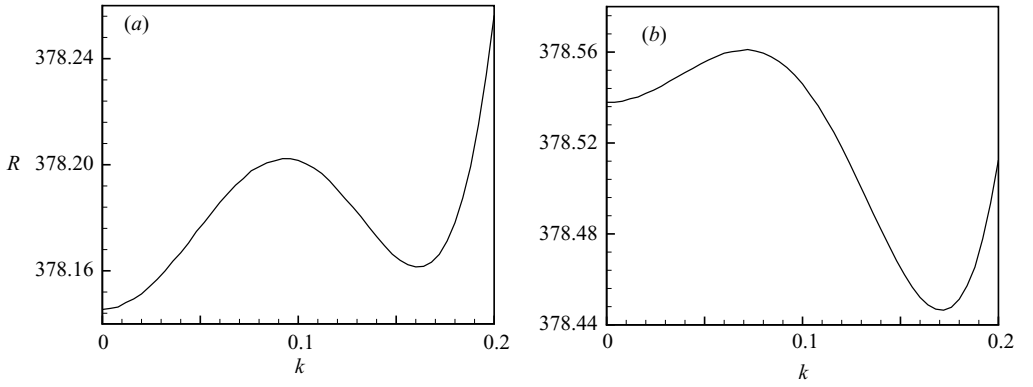

FIGURE 12. Typical neutral curves in the (k, R)-plane for the parameters in the vicinity of the second branch point in figure 11 when surfactant is absent. (a) $\beta = 5.4475$; (b) $\beta = 5.4480$.

agreement of the present results with those in Or (1997). Note that the results reported in the present paper have been calculated at a small β-increment less than 0.1, so that more detailed structures of the curves can be resolved compared with the results of Or (1997, see figure 3 there).

Furthermore, another inconsistency between the present results and Or's is that the second branch point corresponds to a non-zero wavenumber in figure 11(c), similar to the zero-gravity case discussed above. This behaviour was overlooked in Or (1997), because he used only several calculated points to construct the curves. To address this issue, two typical neutral curves in the (k, R)-plane for β near the second branch point are shown in figure 12, similar to figure 4(b) except that the neutral curves emerge from finite values of R at $k = 0$. In particular, both the neutral curves have a local minimum at $k \approx 0.17$. For $\beta = 5.4475$, the lowest minimum is encountered at $k = 0$, and thus long-wavelength disturbances are preferred, while a finite-wavelength instability occurs for $\beta = 5.4480$. This type of switch from the long- to finite-wavelength instabilities differs from that occurring at the first branch point investigated by Or (1997). Considering the Reynolds number R at neutral conditions as a function of k, i.e. $R = R(k)$, Or has suggested that the branch points correspond to where the second-order derivative $R_{kk}(0)$ switches sign. When $R_{kk}(0) > 0$, long-wave instabilities prevail, whereas when $R_{kk}(0) < 0$, finite-wavelength instabilities dominate. Thus, the condition $R_{kk}(0) = 0$ was used to locate the branch points in a long-wave asymptotic analysis. However, this criterion is invalid for the second point shown above, since it is apparent that both the neutral curves in figure 12 have $R_{kk}(0) > 0$, whereas a switch of the stability types may also occur. Strictly speaking, the variation of the second branch point should be determined by accurate numerical solutions instead of the long-wave expansion. In spite of a misleading of stability type, the results of Or (1997, figure 5 there) still provide a reasonably approximate estimation of the location of the second branch point, since the accurate location is very close to asymptotic one.

In the presence of surfactants ($M = 10^{-2}$), the long-wave stability boundaries, denoted by the open-ended loops in figure 11(a,b), are shifted upwards, indicating the long-wave instabilities are suppressed, as revealed by Gao & Lu (2006*a*). Similar to the case in the absence of gravity, the finite-wavelength stability boundaries, corresponding to the travelling-wave modes, branch off the long-wave curves. As β increases to a threshold, instability induced by the standing-wave perturbations takes

over. For sufficiently large values of β, a finite-wavelength stability boundary emanates from a point away from the long-wave boundary owing to large Marangoni number Ma values. Finally, both the stabilizing and destabilizing effects of the surfactants may be observed. Since these features are qualitatively similar to those in the absence of gravity shown above, and the major differences occur in the long-wave region that has been investigated in our previous work (Gao & Lu 2006*a*), the parametric study of the finite-wavelength stability characteristics with respect to M has not been shown in detail here.

4.4. *Eigenfunctions*

For two-layer channel flow with an interfacial surfactant, the Marangoni-induced instability has been interpreted by considering the phase difference between the surfactant concentration and the surface deflection (Frenkel & Halpern 2002; Halpern & Frenkel 2003; Blyth & Pozrikidis 2004*b*). As demonstrated by Wei (2005*b*), this interpretation is only valid for special flow configurations and may lead to inconsistent conclusions for more general conditions. Instead, Wei (2005*b*) proposed an interpretation of the instability of a single-fluid film and a two-fluid channel flow with surfactants, based on disturbance vorticity, which had been used to deal with the surfactant-free film flows (Hinch 1984; Kelly *et al.* 1989; Charru & Hinch 2000). This viewpoint is appropriate because the instability may occur either at low Reynolds numbers, indicating weak inertial effects, or at large wavelength regimes, resulting in a uniform distribution of the disturbance vorticity across the fluid layer. However, it is not appropriate for the oscillatory flow considered here. Indeed, no obvious relations between the disturbance vorticity and the surface deformation can be obtained based on our calculations. Essentially, it is due to spatially distributed mass flow rate induced by the disturbance vorticity causing the growth or decaying of the surface deflection. Another aspect to identify the stability of the flow is the accumulation and the dilution of surfactant, induced by advective effects of the streamwise perturbation velocity, $u'(x, 0, t)$, at the surface. Gao & Lu (2006*a*) have shown that the growth (decaying) of the amplitudes of the surface wave and the surfactant wave is related to positive (negative) phase differences, i.e. $\mathrm{Arg}(\phi(0)/h)$ and $\mathrm{Arg}(\phi_y(0)/\xi)$, where $\phi(0, t)$ and $\phi_y(0, t)$ are the complex amplitudes of the mass flow rate across the fluid layer and perturbating surface velocity $u'(x, 0, t)$, respectively. These interpretations can also be applied to the finite-wavelength stabilities.

Typical critical modes through a modulation cycle are shown in figure 13 for $\chi = 0$, $\psi = 0.05$ and $M = 10^{-3}$. The values of β are specified to be 3.0 and 3.2, as shown in figure 5, corresponding to the travelling- and standing-wave instabilities, respectively. The critical mode in the form of travelling wave is associated with the eigenvalue $\mu = 0.08\mathrm{i}$. The disturbance streamfunctions are shown in figure 13(*a*, *b*) by the contours of $|\hat{\phi}(y, t)|$. The primary activity of the disturbance flow occurs in a layer adjacent to the free surface as expected. The variations of the amplitudes of surface wave and surfactant concentration wave, together with the phase differences $\mathrm{Arg}(\phi(0)/h)$ and $\mathrm{Arg}(\phi_y(0)/\xi)$, are shown in figures 13(*c*, *d*) and 13(*e*, *f*), respectively. Note that the eigenfunctions are normalized by

$$\int_0^{2\pi} \hat{h}(t)\,\mathrm{d}t = 1.$$

It is clear that the positive (negative) $\mathrm{Arg}(\phi(0)/h)$ corresponds to the growth (decaying) of $|\hat{h}|$, so is the relation between $\mathrm{Arg}(\phi_y(0)/\xi)$ and $|\hat{\xi}|$, in accordance with Gao & Lu (2006*a*). The phase differences between the surfactant concentration

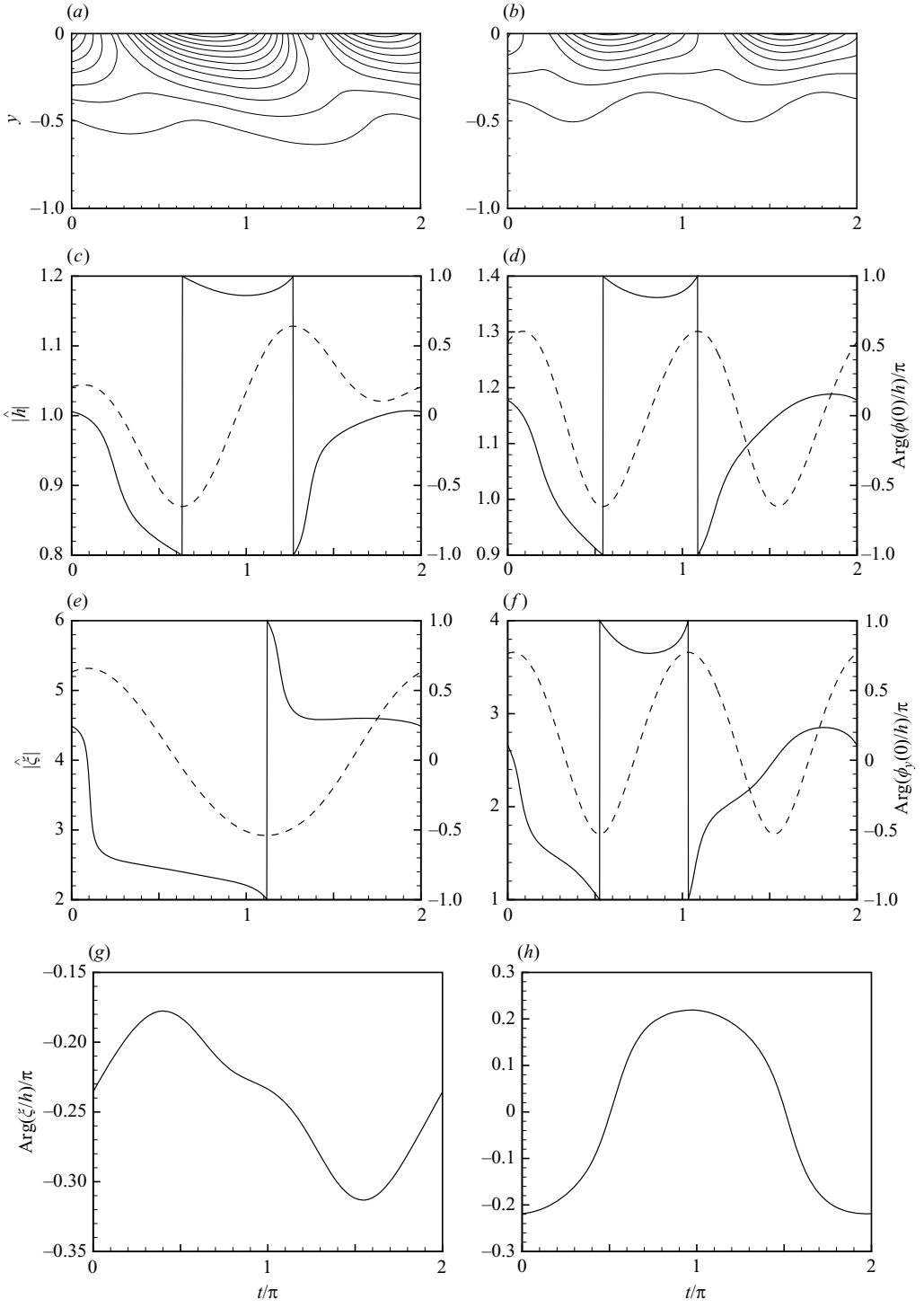

FIGURE 13. Properties of typical critical modes over a period for $\chi = 0$, $\psi = 0.05$ and $M = 10^{-3}$. Results in the left-hand column are obtained at $\beta = 3$, corresponding to a travelling-wave mode with $\mu = 0.08$i. Results in the right-hand column are calculated at $\beta = 3.2$, corresponding to a standing-wave mode. (a, b) the contours of $|\hat{\phi}(y, t)|$ with an interval of 0.01. The phase differences, defined on $[-\pi, \pi]$, and the amplitudes of the eigenfunctions are denoted by the solid and dashed lines, respectively.

wave and the surface wave are exhibited in figure 13(g, h). It is found that the values of Arg(ξ/h) are always negative for the travelling-wave modes, and vary around zero for the standing-wave modes. The occurrence of the standing modes can be explained as follows. If the surfactant concentration wave induces the surface wave to propagate to the right at an instant t_0, it makes the surface wave propagate to the left at $t_0 + \pi$, owing to an opposite phase difference. Hence the mode has a form of standing wave in the sense of averaging over one period.

5. Concluding remarks

The linear stability of a fluid layer driven by an oscillating plate and covered by an insoluble surfactant has been investigated for disturbances of arbitrary wavenumbers with a wide range of amplitude and frequency of the modulation as well as surfactant elasticity. Our extensive results show that finite-wavelength instability may not only occur, but also can be more unstable than the long waves. Thus, considering only the stability characteristics of long-wave disturbances, as in Gao & Lu (2006*a*), is insufficient to determine the final fate of the system. Further, the finite-wavelength stability characteristics of the flow with and without gravity are qualitatively similar to each other, while major differences exist in the long-wave instabilities. Thus, the finite-wavelength instabilities of the zero-gravity case are elucidated in detail, while those in the presence of gravity are similar.

The occurrence of either long- or finite-wavelength instabilities depends primarily on the amplitude and frequency of the modulation, characterized by R and β, respectively. In the absence of gravity, the long-wave instability occurs for alternative bandwidths of frequency, and the deformation of the surface grows exponentially once the modulations with non-zero amplitude are imposed, i.e. $R > 0$. Otherwise, for the frequencies where long waves are damped, the finite-wavelength instability arises for sufficiently large amplitudes of the modulation, i.e. $R > R_c > 0$. Thus, the transition from the long- to finite-wavelength instabilities with increasing frequency occurs in a discontinuous way. In addition, the two types of instability can coexist for some ranges of frequency, and the competition between them always results in the dominance of long waves. Generally, the critical Reynolds number R_c increases with the imposed frequency so that the stability boundaries associated with the finite-wavelength instability exhibit a monotonically increasing behaviour. A qualitative interpretation can be given as the modulation with a high frequency may cause a thinner Stokes layer near the wall and therefore a weaker basic flow near the surface, which can be reinforced by increasing the amplitude of the oscillation to destabilize the flow, leading to a higher critical Reynolds number.

The major finding of the present study is that the presence of surfactants can either stabilize or destabilize the instability of the flow depending on the strength of the surface elasticity. It is found in Gao & Lu (2006*a*) that the effect of surfactants is always stabilizing for long waves. However, the critical Reynolds number can be either raised or lowered by the surfactants depending on the parameters, so both stabilizing and destabilizing effects of surfactants are detected in the current work. Generally, for a weak surface elasticity, which is characterized by the dimensionless number M, the stabilization of the flow is encountered, as also found extensively in steady-flow systems with a free surface; whereas for a large surface elasticity, the presence of surfactants tends to destabilize the flow. Note that the destabilizing effect of surfactants has never been found in free-surface flow systems. In addition, different from the clean-surface case (Or 1997), in which the critical modes have the form of

standing waves, instabilities dominated by the travelling-wave modes can also occur here. The corresponding wavenumbers of the travelling-wave branch of the neutral curve are larger than those of the standing-wave branch for a group of parameters. In addition, the variation of the critical wavenumber along each finite-wavelength boundary exhibits a strongly non-monotonic feature compared with the clean surface case. As the imposed frequency increases, the preferred wavenumber may switch from one branch to the other in a discontinuous way.

In the present problem, the stability of the flow is determined by two coupled Floquet modes associated with the surface deformation and the Marangoni force. The travelling-wave modes are related to the eigenvalues which are complex conjugate to each other, and therefore $\mu_i \neq 0$. We emphasize that the occurrence of travelling-wave modes does not conflict with the results of Or (1997) for an oscillatory clean-surface flow, wherein the neutral modes always have the form of standing waves, i.e. $\mu_i = 0$. Or (1997) has demonstrated the non-existence of subharmonic solutions ($\mu_i = 1/2$) in a shear-modulated system. However, this argument does not exclude the possibility of the existence of quasi-periodic solutions for $0 < \mu_i < 1/2$. Indeed, our extensive examination of the travelling-wave solutions indicates that μ_i is always less than $1/2$, consistent with Or's results.

The results have been shown for $\beta < 10$ in this paper. For higher values of frequencies, the modulation-induced Stokes layer is confined in a very thin region adjacent to the plate. Thus, the influence of the modulation on the dynamics of the surface is weak and the growth rate of the disturbance modes is exponentially small. In this situation, the round-off error begins to pollute the eigenvalues, leading to difficulties in the investigations of the instability caused by the free surface at high frequencies. On the other hand, for sufficiently high frequencies, the shear modes associated with the underlying basic velocity profile may dominate the stability characteristics, which should tend to that of plane Stokes layers (Blennerhassett & Bassom 2002; Gao & Lu 2006*b*; Blennerhassett & Bassom 2006). This type of instability has been studied using a more appropriate definition of the Reynolds number based on the thickness of Stokes layers.

This work was supported by the Innovation Funds of Graduates at USTC, the National Natural Science Foundation of China (nos. 90405007 and 10332040), the Hundred Talents Program of the Chinese Academy of Sciences, and Program for Changjiang Scholars and Innovative Research Team in University.

Appendix. The limit of $R \to 0$

As the Reynolds number R tends to zero with fixed M, an analytical solution of the differential system (2.7) to (2.12) can be represented as

$$\phi(y,t) = \phi_0(y,t) + R\phi_1(y,t) + \cdots, \tag{A 1}$$

$$h(t) = Rh_1(t) + \cdots, \quad \xi(t) = \xi_0(t) + R\xi_1(t) + \cdots. \tag{A 2}$$

The leading-order system is

$$2\beta^2 \frac{\partial}{\partial t}\left(\frac{\partial^2}{\partial y^2} - k^2\right)\phi_0 = \left(\frac{\partial^2}{\partial y^2} - k^2\right)^2 \phi_0, \tag{A 3}$$

subject to the boundary conditions

$$\phi_0 = \frac{\partial \phi_0}{\partial y} = 0 \quad \text{at} \quad y = -1, \tag{A 4}$$

and

$$2\beta^2 \frac{\partial^2 \phi_0}{\partial t \partial y} - \left(\frac{\partial^2}{\partial y^2} - 3k^2 \right) \frac{\partial \phi_0}{\partial y} + \mathrm{i}k \left(2\chi + \frac{k^2}{\psi} \right) h_1 = 0, \tag{A 5}$$

$$\frac{\partial^2 \phi_0}{\partial y^2} + k^2 \phi_0 = 0, \tag{A 6}$$

$$2\beta^2 \frac{\partial h_1}{\partial t} + \mathrm{i}k\phi_0 = 0 \quad \text{at} \quad y = 0. \tag{A 7}$$

It can be seen that ξ_0 does not enter the boundary conditions for ϕ_0 and hence the surfactant transport equations is not required.

Since the coefficients of the system are independent of t, we can express ϕ_0 and h_1 as

$$\phi_0(y, t) = \mathrm{e}^{\mu t} \Upsilon(y), \quad h_1(t) = \mathrm{e}^{\mu t} \theta. \tag{A 8}$$

Substituting (A 8) into (A 3) yields

$$\left(\frac{\mathrm{d}^2}{\mathrm{d}y^2} - \gamma^2 \right) \left(\frac{\mathrm{d}^2}{\mathrm{d}y^2} - k^2 \right) \Upsilon = 0, \tag{A 9}$$

which is solved with the conditions

$$\Upsilon(-1) = \frac{\mathrm{d}\Upsilon}{\mathrm{d}y}(-1) = 0, \tag{A 10}$$

$$(\gamma^2 + 2k^2) \frac{\mathrm{d}\Upsilon}{\mathrm{d}y}(0) - \frac{\mathrm{d}^3 \Upsilon}{\mathrm{d}y}(0) + \frac{k^2}{\gamma^2 - k^2} \left(2\chi + \frac{k^2}{\psi} \right) \Upsilon(0) = 0, \tag{A 11}$$

$$\frac{\mathrm{d}^2 \Upsilon}{\mathrm{d}y^2}(0) + k^2 \Upsilon(0) = 0, \tag{A 12}$$

where $\gamma^2 = 2\beta^2 \mu + k^2$. When deriving tangential stress condition (A 11), the kinematic condition $\theta = -\mathrm{i}k\Upsilon/(\gamma^2 - k^2)$ has been used. The general solution of (A 9) has the form

$$\Upsilon(y) = C_1 \cosh \gamma y + C_2 \sinh \gamma y + C_3 \cosh ky + C_4 \sinh ky, \tag{A 13}$$

where the coefficients C_j $(j = 1, 2, 3, 4)$ are determined by the boundary conditions, and can be given in the matrix form

$$\begin{pmatrix} \cosh \gamma & -\sinh \gamma & \cosh k & -\sinh k \\ -\gamma \sinh \gamma & \gamma \cosh \gamma & -k \sinh k & k \cosh k \\ \dfrac{k^2}{\gamma^2 - k^2} \left(2\chi + \dfrac{k^2}{\psi} \right) & 2\gamma k^2 & \dfrac{k^2}{\gamma^2 - k^2} \left(2\chi + \dfrac{k^2}{\psi} \right) & k(\gamma^2 + k^2) \\ \gamma^2 + k^2 & 0 & 2k^2 & 0 \end{pmatrix} \begin{pmatrix} C_1 \\ C_2 \\ C_3 \\ C_4 \end{pmatrix} = \mathbf{0}. \tag{A 14}$$

The existence of a non-trivial solution requires the determinant of the coefficient matrix to be zero, which produces an infinite family of γ and therefore μ. In general, both purely real and complex eigenvalues are found, different from the well-known Dolph–Lewis eigenvalues (Dolph & Lewis 1958).

REFERENCES

Blennerhassett, P. J. & Bassom, A. P. 2002 The linear stability of flat Stokes layers. *J. Fluid Mech.* **464**, 393–410.

Blennerhassett, P. J. & Bassom, A. P. 2006 The linear stability of high-frequency oscillatory flow in a channel. *J. Fluid Mech.* **556**, 1–25.

Blyth, M. G. & Pozrikidis, C. 2004*a* Effect of surfactant on the stability of film flow down an inclined plane. *J. Fluid Mech.* **521**, 241–250.

Blyth, M. G. & Pozrikidis, C. 2004*b* Effect of surfactants on the stability of two-layer channel flow. *J. Fluid Mech.* **505**, 59–86.

Canuto, C., Hussaini, M. Y., Quarteroni, A. & Zang, T. A. 1988 *Spectral Methods in Fluid Dynamics*. Springer.

Charru, F. & Hinch, E. J. 2000 'Phase diagram' of interfacial instabilities in a two-layer Couette flow and mechanism of the long-wave instability. *J. Fluid Mech.* **414**, 195–223.

Coward, A. V. & Papageorgiou, D. T. 1994 Stability of oscillatory two-phase Couette flow. *IMA J. Appl. Maths* **53**, 75–93.

Coward, A. V. & Renardy, Y. Y. 1997 Small-amplitude oscillatory forcing on two-layer plane channel flow. *J. Fluid Mech.* **334**, 87–109.

Dolph, C. L. & Lewis, D. C. 1958 On the application of infinite systems of ordinary differential equations to perturbations of plane Poiseuille flow. *Q. Appl. Maths* **16**, 97–110.

Fornberg, B. 1996 *A Practical Guide to Pseudospectral Methods*. Cambridge University Press.

Frenkel, A. L. & Halpern, D. 2002 Stokes-flow instability due to interfacial surfactant. *Phys. Fluids* **14**, L45–L48.

Frenkel, A. L. & Halpern, D. 2005 Effect of inertia on the insoluble-surfactant instability of a shear flow. *Phys. Rev.* E **71**, 016302.

Gao, P. & Lu, X.-Y. 2006*a* Effect of surfactants on the long-wave stability of oscillatory film flow. *J. Fluid Mech.* **562**, 345–354.

Gao, P. & Lu, X.-Y. 2006*b* Effects of wall suction/injection on the linear stability of flat Stokes layers. *J. Fluid Mech.* **551**, 303–308.

Gao, P. & Lu, X.-Y. 2006*c* Instability of channel flow with oscillatory wall suction/blowing. *Phys. Fluids* **18**, 034102.

Gao, P. & Lu, X.-Y. 2007 Effect of surfactants on the inertialess instability of a two-layer film flow. *J. Fluid Mech.* **591**, 495–507.

Halpern, D. & Frenkel, A. L. 2001 Saturated Rayleigh–Taylor instability of an oscillating Couette film flow. *J. Fluid Mech.* **446**, 67–93.

Halpern, D. & Frenkel, A. L. 2003 Destabilization of a creeping flow by interfacial surfactant: linear theory extended to all wavenumbers. *J. Fluid Mech.* **485**, 191–220.

Hinch, E. J. 1984 A note on the mechanism of the instability at the interface between two shearing flows. *J. Fluid Mech.* **144**, 463–465.

Kelly, R. E., Goussis, D. A., Lin, S. P. & Hsu, F. K. 1989 The mechanism for surface wave instability in film flow down an inclined plane. *Phys. Fluids* A **1**, 819–828.

von Kerczek, C. & Davis, S. H. 1974 Linear stability theory of oscillatory Stokes layers. *J. Fluid Mech.* **62**, 753–773.

King, M. R., Leighton, D. T. & McCready, M. J. 1999 Stability of oscillatory two-phase Couette flow: theory and experiment. *Phys. Fluids* **11**, 833–844.

Li, X. F. & Pozrikidis, C. 1997 The effect of surfactants on drop deformation and on the rheology of dilute emulsions in Stokes flow. *J. Fluid Mech.* **341**, 165–194.

Lin, S. P. 1970 Stabilizing effects of surface-active agents on a film flow. *AIChE J.* **16**, 375–379.

Or, A. C. 1997 Finite-wavelength instability in a horizontal liquid layer on an oscillating plane. *J. Fluid Mech.* **335**, 213–232.

Or, A. C. & Kelly, R. E. 1998 Thermocapillary and oscillatory-shear instabilities in a layer of liquid with a deformable surface. *J. Fluid Mech.* **360**, 21–39.

Ostrach, S. 1982 Low-gravity fluid flows. *Annu. Rev. Fluid. Mech.* **14**, 313–345.

Phillips, W. R. C. 2001 On an instability to Langmuir circulations and the role of Prandtl and Richardson numbers. *J. Fluid Mech.* **442**, 335–358.

Pozrikidis, C. 2003 Effect of surfactants on film flow down a periodic wall. *J. Fluid Mech.* **496**, 105–127.

Sarpkaya, T. 1996 Vorticity, free surface, and surfactants. *Annu. Rev. Fluid. Mech.* **28**, 83–128.

Shen, L., Yue, D. K. P. & Triantafyllou, G. S. 2004 Effect of surfactants on free-surface turbulent flows. *J. Fluid Mech.* **506**, 79–115.

Skarda, J. R. L. 2001 Instability of a gravity-modulated fluid layer with surface tension variation. *J. Fluid Mech.* **434**, 243–271.

Stone, H. A. 1990 A simple derivation of the time-dependent convection–diffusion equation for surfactant transport along a deforming interface. *Phys. Fluids* A **2**, 111–112.

Thiele, U., Vega, M. & Knobloch, E. 2006 Long-wave Marangoni instability with vibration. *J. Fluid Mech.* **546**, 61–87.

Wei, H.-H. 2005*a* Effect of surfactant on the long-wave instability of a shear-imposed liquid flow down an inclined plane. *Phys. Fluids* **17**, 012103.

Wei, H.-H. 2005*b* On the flow-induced Marangoni instability due to the presence of surfactant. *J. Fluid Mech.* **544**, 173–200.

Wei, H.-H., Halpern, D. & Grotberg, J. B. 2005 Linear stability of a surfactant-laden annular film in a time-periodic pressure-driven flow through a capillary. *J. Colloid Interface Sci.* **285**, 769–780.

Weideman, J. A. C. & Reddy, S. C. 2000 A matlab differentiation matrix suite. *ACM Trans. Math. Software* **26**, 465–519.

Whitaker, S. & Jones, L. O. 1966 Stability of falling liquid films. Effect of interface and interfacial mass transport. *AIChE J.* **12**, 421–431.

Wong, H., Rumschitzki, D. & Maldarelli, C. 1996 On the surfactant mass balance at a deforming fluid interface. *Phys. Fluids* **8**, 3203–3204.

Yih, C. S. 1963 Stability of liquid flow down an inclined plane. *Phys. Fluids* **6**, 321–334.

Yih, C. S. 1968 Instability of unsteady flows or configurations. Part 1. Instability of a horizontal liquid layer on an oscillating plane. *J. Fluid Mech.* **31**, 737–751.